PHYSICAL REVIEW B VOLUME 27, NUMBER 7 1 APRIL 1983

Strain-modulated ESR study of Pt^- in silicon

J. C. M. Henning and E. C. J. Egelmeers
Philips Research Laboratories, 5600-JA Eindhoven, The Netherlands
(Received 10 May 1982; revised manuscript received 10 December 1982)

Early electron-spin-resonance (ESR) studies by Woodbury and Ludwig on the Pt acceptor in Si have been refined and extended. The strain dependence of the spectroscopic splitting tensor $\vec{g}$ has been measured using the strain-modulated electron-spin-resonance technique. The symmetry of the center proves to be monoclinic. The 20 independent elements of the magnetoelastic tensor $\vec{F}$ allowed in C_s symmetry are determined at $T=4.2$ K. New details in the ESR spectra are also reported. A superhyperfine structure due to a second Pt atom indicates that Pt enters the lattice as pairs. Experiments on samples with varying Pt and P concentrations show that in the concentration range $10^{16}<[\mathrm{Pt}]<10^{17}\ \mathrm{cm}^{-3}$, Pt is exclusively present as Pt^--Pt^0 pairs. Single Pt^- centers are not observed. The doubly charged pair state Pt^--Pt^- is also absent, even in samples with high [P]/[Pt] ratio. This implies that both members of the pair must be located at distinct types of sites. The following model accounts for all observed features: One of the platinums (Pt^-) is at a near-substitutional site. It forms chemical bonds with two neighboring silicon atoms and is shifted in their direction along a [001] axis. The remaining two silicon neighbors form a reconstructed bond. The second Pt^0 atom is at an interstitial site; its presence is responsible for the monoclinic (C_s) center symmetry.

I. INTRODUCTION

The introduction of heavy metals such as gold and platinum is a common way of controlling lifetimes of both electron and hole carriers in silicon. Although a wealth of macroscopic experimental data is available relating to the capture process,[1-5] the microscopic structure of the deep centers involved is still uncertain.

Detailed information about the structure of the centers can, in principle, be obtained from electron-spin resonance (ESR) and optical spectroscopy.[6] With respect to the system Si:Pt, however, the spectroscopic data are scant. Electron-spin resonance in Pt-doped n-type silicon has been reported by Woodbury and Ludwig.[7] Two paramagnetic species were observed, both with spin $\frac{1}{2}$. The first Pt center has orthorhombic symmetry and was attributed to the singly charged, substitutional Pt^- center (acceptor). Its resonance signal disappears above 12 K. The second spectrum with axial symmetry along $\langle 111 \rangle$ was observed at 20 K and higher. Its intensity varied from sample to sample and showed some correlation with the oxygen content. Both centers act as hole traps; the longer trapping time at 10 K suggests that the axial center might be a double acceptor.[7] The structure of the axial center is not further discussed in Ref. 7.

Concerning the orthorhombic center three possible suggestions were made:

(i) Four of the eleven available valence electrons of Pt^- are used to complete the tetrahedral bonding with four nearest neighbors. The d shell contains eight electrons and is diamagnetic. There is, however, a bound hole in a $j=\frac{3}{2}$ state localized about the impurity ion. The remaining electronic degeneracy is lifted by a Jahn-Teller distortion in the [001] direction.

(ii) Chemical bonds are formed with two of the four Si neighbors (analogous to the silicon A center[8,9]). The remaining two silicon atoms form a "reconstructed bond." The d shell contains eight electrons, which are paired off. An unpaired electron occupies the antibonding orbital of the reconstructed bond.

(iii) As in case (ii) there is chemical bonding with two silicon neighbors. Paramagnetism, however, now arises from the d shell, which contains nine electrons. The antibonding orbital of the reconstructed Si—Si bond is empty.

In Woodbury and Ludwig's paper a definite decision between these three possibilities is not made, although the authors seem to have a slight preference for case (iii). A recent 17-atoms cluster calculation by Lowther[10] leads to a picture which is essentially identical with case (ii).

The investigations described in the present paper were devised to obtain more information about the physical nature of the Pt^- center. To this end ESR measurements have been refined and extended with strain-modulated electron-spin-resonance (SMESR) results.[11] The SMESR technique has already been used with success to detect the Pt^+ center in p-type Si.[12] The novel information obtained here is the strain dependence of the spectroscopic splitting tensor: $\overleftrightarrow{g}=\overleftrightarrow{F}\cdot\overleftrightarrow{e}$. It follows unambiguously from the experiments that the site symmetry is monoclinic (C_s) instead of orthorhombic. The 20 independent elements of the magnetoelastic coupling tensor $\overleftrightarrow{F}$ allowed in C_s symmetry are determined at $T=4.2$ K. A new detail in the ESR spectra is the presence of hyperfine structure due to a second Pt^0 atom. Finally, the number of ESR-active centers equals just half the total Pt content. These new experimental facts lead unambiguously to the conclusion that the Pt acceptor in Si is not an isolated ion, but a Pt^--Pt^0 pair.

A plausible model of the Pt^--Pt^0 center will be deduced in Sec. VI. The experiments are presented in Sec. V, preceded by a mathematical section (Sec. IV) on the evaluation of the $\overleftrightarrow{F}$-tensor elements in monoclinic symmetry. A description of the samples used and of the experimental setup is given in Secs. III and II, respectively.

II. SMESR DETAILS

SMESR is a variant of the ESR technique in which differential sensing of the spectral lines is accomplished by modulating the internal crystal field. The method was introduced ten years ago by Badalian and Kazantsev[13] and was soon thereafter taken over by other workers.[14–16] It is particularly suited to the study of deep centers in semiconductors, where, as a consequence of the strong spin-lattice coupling, large modulation depths can be attained with moderate strain amplitudes. An extreme example is the Pt^+ center in Si,[12] where F figures of the order of 2×10^4 are reported. In order to illustrate the dynamic range of the SMESR method we mention that the F values of Cr^{3+} in MgO are of the order of 10^{-2}.[11]

For the present investigations a conventional X-band (10 GHz) homodyne mixer spectrometer was equipped with both magnetic field (419 Hz) and strain-modulation (108 kHz) facilities. ESR and SMESR spectra were recorded simultaneously. Details of the setup are given elsewhere.[11] The silicon samples, cut into blocks with dimensions $2\times2\times2$ mm^3 or $2\times2\times5$ mm^3, were mounted onto the electromechanical transducer using Stycast 2850 FT (Emerson and Cuming, Inc.) as an adhesive. The composite transducer was operated in the $\frac{3}{2}\lambda$ longitudinal extensional mode, at 108 kHz. The stress axis coincided with either of the crystal axes [111], [110], [001], or [11$\bar{2}$]. The magnetic field vector $\vec{H}$ could be rotated in a plane perpendicular to the stress axis. As a rule, measurements were carried out at $T=4.2$ K. At this temperature, the spin-lattice relaxation time of Pt^- proved to be sufficiently short to operate the spectrometer in the absorption mode. Essentially slow passage conditions could be maintained up to 108 kHz.

III. SAMPLES

Platinum-doped silicon samples were provided by Dr. S. D. Brotherton (Philips Research Laboratory, Redhill, United Kingdom). The bulk of the measurements reported in this paper was done on samples prepared from float-zoned n^+-type silicon. Platinum diffusion was carried out at 1200 °C for 64 h in N_2 atmosphere. The resistivity of the starting material was 0.017 Ω cm; after Pt diffusion a value of 0.022 Ω cm was measured. An estimate of the P concentration can be obtained either from the electric resistivity, 1.3×10^{18} cm^{-3}, or from the ESR linewidth of the phosphorous resonance signal, 8×10^{17} cm^{-3}.[17] The total Pt content was determined by neutron activation analysis: $[Pt]=1.08\times10^{17}$ cm^{-3}. Further impurities are the following: Ni (120), Cu (710), Te (24), and Ba (22); here, the figures in parentheses are parts per 10^9 by weight. The oxygen concentration was determined by means of infrared spectroscopy and amounts to $[O]=5\times10^{16}$ cm^3.

Some additional measurements were carried out on Czochralski material with $[P]=8.3\times10^{16}$ cm^{-3}, $[O]=6\times10^{17}$ cm^{-3}, and a varying Pt concentration: 1.7×10^{16} $cm^{-3}<[Pt]<6.6\times10^{16}$ cm^{-3}. In these samples the Pt concentration was high enough to observe ESR spectra and low enough to carry out deep-level transient-spectroscopy (DLTS) measurements.[18] The latter show one peak close to the temperature where, in more dilute (10^{14}–10^{15} cm^{-3}) samples, the "normal" Pt^- acceptor peak is found. We therefore conclude that our ESR measurements actually refer to the Pt acceptor at $E_t=E_c-0.23$ eV.

Control ESR measurements were always carried out on undoped samples, which had undergone the same heat treatment as the doped ones. After cutting, all specimens were eteched in a $HF+HNO_3$ mixture in order to remove surface impurities which give an ESR signal at $g=2.0055$.

IV. EVALUATION OF THE $\overleftrightarrow{F}$ TENSOR

Application of stress to a solid sample containing paramagnetic centers may, in principle, give rise to a

TABLE I. Equivalent Pt^- centers.

	x	y	z
A	$[1\bar{1}0]$	$[110]$	$[001]$
B	$[110]$	$[\bar{1}10]$	$[001]$
C	$[011]$	$[0\bar{1}1]$	$[100]$
D	$[0\bar{1}1]$	$[0\bar{1}\bar{1}]$	$[100]$
E	$[\bar{1}01]$	$[101]$	$[010]$
F	$[101]$	$[10\bar{1}]$	$[010]$

variety of effects:

(i) The parameters of the spin Hamiltonian may change, resulting in a shift and/or a splitting of the resonance lines.

(ii) The spin-lattice relaxation time T_1 may change, resulting in a modified linewidth.

(iii) A redistribution among various charge states of the centers may occur.

(iv) The centers themselves may reorient. The latter two effects give rise to a modification of the intensity ratios in the ESR spectrum. They belong to the class of anelastic effects and commonly occur on a time scale which is large compared with the SMESR modulation period. To be more specific, for the A center (oxygen vacancy) in silicon—which shows some similarity with the Pt center studied here—charge redistribution has been observed[8] for 60 K $< T <$ 70 K with characteristic times between 5 and 1000 sec, and reorientation times of the same order are reported in the temperature range 120–150 K. Hence for $T = 4.2$ K and SMESR frequencies in the vicinity of 100 kHz, anelastic effects are expected to play a negligible role. The purely elastic effects (i) and (ii) are characterized by the fact that the SMESR signals are in phase with the driving strain. They can be distinguished on account of the observed line shape. Modulation of the relaxation time will lead to an absorption line shape, whereas the shape of shift-SMESR signals resembles the first derivative of absorption (provided that the modulation depth is small compared with the linewidth).

Anticipating some qualitative results of Sec. V, we now derive the equations needed in evaluating the SMESR data. It turns out that SMESR signals due to the Pt^- center in Si belong to class (i). The centers have a spin $S = \frac{1}{2}$ and monoclinic symmetry (point group C_s). However, the typical monoclinic element g_{xz} of the spectroscopic splitting tensor proves to be vanishingly small. Hence it still makes sense to speak of an orthorhombic set of principal center axes (x,y,z). One particular center (A) has principal axes along $x = [1\bar{1}0]$, $y = [110]$, $z = [001]$. It is reproduced six times by the symmetry operations of the cubic crystal class. The six equivalent centers are labeled A, B, C, D, E, and F (Table I).

The main effect of the periodic strain field is modulation of the spectroscopic splitting tensor. For small strains we may write

$$\begin{vmatrix} \delta g_{xx} \\ \delta g_{yy} \\ \delta g_{zz} \\ \delta g_{yz} \\ \delta g_{zx} \\ \delta g_{xy} \end{vmatrix} = \begin{vmatrix} F_{11} & F_{12} & F_{13} & 0 & F_{15} & 0 \\ F_{21} & F_{22} & F_{23} & 0 & F_{25} & 0 \\ F_{31} & F_{32} & F_{33} & 0 & F_{35} & 0 \\ 0 & 0 & 0 & F_{44} & 0 & F_{46} \\ F_{51} & F_{52} & F_{53} & 0 & F_{55} & 0 \\ 0 & 0 & 0 & F_{64} & 0 & F_{66} \end{vmatrix} \begin{vmatrix} e_{xx} \\ e_{yy} \\ e_{zz} \\ e_{yz} \\ e_{zx} \\ e_{xy} \end{vmatrix} , \tag{1}$$

where the magnetoelastic coupling tensor $\overleftrightarrow{F}$ has a form appropriate to C_s symmetry with the principal axis along y. It contains 20 nonvanishing elements. Note that the strains used throughout this paper are the engineering strains.

Our experimental setup allows a rotation of the magnetic field vector $\vec{H}$ in a plane perpendicular to the stress axis $\vec{T}$. The stress axis is chosen along a crystallographic direction with simple indices, e.g., [001], [111], [110], or $[11\bar{2}]$. For specific orientations of $\vec{T}$ and $\vec{H}$, effective F_H^T values are measured by comparing the SMESR signal heights I_s with the heights of the H-modulated ESR signals I_e. If the gains of the SMESR (G_s) and ESR (G_e) spectrometers are known, an effective strain-modulation amplitude $\hat{m}_s$ is found from

$$\hat{m}_s = \hat{m}_e (I_s / I_e)(G_e / G_s) , \tag{2}$$

where $\hat{m}_e$ is the magnetic field modulation amplitude. This equation has to be corrected for passage effects, due to the difference in modulation frequencies used in the SMESR (108 kHz) and ESR (419 Hz) spectrometers.[19] The effective F_H^T value follows from

$$F_H^T = \frac{g\hat{m}_s}{H\hat{e}_s} , \tag{3}$$

where g is the effective static g value and $\hat{e}_s$ is the strain-modulation amplitude.

Our present task is to correlate the effective F_H^T values with the tensor elements F_{ij}. For a particular center (A) a general relationship is easily derived. Let (τ_1, τ_2, τ_3) be the direction cosines of the stress $\vec{T}$

with respect to the cubic axes (ξ,η,ζ); the direction cosines of $\vec{H}$ with respect to the principal axes (x,y,z) of center A are denoted by $(\alpha_1,\alpha_2,\alpha_3)$.

The perturbation induced by strain modulation is described by the spin Hamiltonian

$$\tilde{\mathcal{H}}=\mu_B H_\alpha \delta g_{\alpha\beta} S_\beta \,, \tag{4}$$

where $\delta g_{\alpha\beta}$ are given by Eq. (1). First-order energy shifts are produced by spin components $S_{||}$ parallel with $\vec{H}$. This leads to a truncated spin Hamiltonian

$$\tilde{\mathcal{H}}_{\rm tr}=\mu_B H(\alpha_1^2\delta g_{xx}+\alpha_2^2\delta g_{yy}+\alpha_3^2\delta g_{zz}+2\alpha_1\alpha_2\delta g_{xy}+2\alpha_2\alpha_3\delta g_{yz}+2\alpha_3\alpha_1\delta g_{xz})S_{||}\equiv\mu_B H F_H^T \hat{e}_s S_{||} \,. \tag{5}$$

In order to evaluate the $\delta g_{\alpha\beta}$ $(\alpha,\beta=x,y,z)$ we take the following steps: (1) evaluation of the strains in the cubic system (ξ,η,ζ), using the cubic compliance tensor s_{kl} of silicon; (2) transformation of the strains to the Cartesian axes of a center (x,y,z) (Ref. 20); (3) application of Eq. (1), which then leads to the following results:

$$\begin{aligned}
\delta g_{xx}&=\{F_{11}[s_{11}+s_{12}-(s_{11}-s_{12})\tau_3^2-s_{44}\tau_1\tau_2]+F_{12}[s_{11}+s_{12}-(s_{11}-s_{12})\tau_3^2+s_{44}\tau_1\tau_2]\\
&\quad+F_{13}[2s_{12}+2(s_{11}-s_{12})\tau_3^2]+F_{15}\sqrt{2}s_{44}(\tau_1-\tau_2)\tau_3\}\frac{T}{2}\,,\\
\delta g_{yy}&=\{F_{21}[s_{11}+s_{12}-(s_{11}-s_{12})\tau_3^2-s_{44}\tau_1\tau_2]+F_{22}[s_{11}+s_{12}-(s_{11}-s_{12})\tau_3^2+s_{44}\tau_1\tau_2]\\
&\quad+F_{23}[2s_{12}+2(s_{11}-s_{12})\tau_3^2]+F_{25}\sqrt{2}s_{44}(\tau_1-\tau_2)\tau_3\}\frac{T}{2}\,,\\
\delta g_{zz}&=\{F_{31}[s_{11}+s_{12}-(s_{11}-s_{12})\tau_3^2-s_{44}\tau_1\tau_2]+F_{32}[s_{11}+s_{12}-(s_{11}-s_{12})\tau_3^2+s_{44}\tau_1\tau_2]\\
&\quad+F_{33}[2s_{12}+2(s_{11}-s_{12})\tau_3^2]+F_{35}\sqrt{2}s_{44}(\tau_1-\tau_2)\tau_3\}\frac{T}{2}\,,\\
\delta g_{yz}&=F_{44}\tfrac{1}{2}\sqrt{2}s_{44}(\tau_1+\tau_2)\tau_3 T+F_{46}(s_{11}-s_{12})(\tau_1^2-\tau_2^2)T\,,\\
\delta g_{zx}&=F_{55}\tfrac{1}{2}\sqrt{2}s_{44}(\tau_1-\tau_2)\tau_3 T+\{F_{51}[s_{11}+s_{12}-(s_{11}-s_{12})\tau_3^2-s_{44}\tau_1\tau_2]\\
&\quad+F_{52}[s_{11}+s_{12}-(s_{11}-s_{12})\tau_3^2+s_{44}\tau_1\tau_2]+F_{53}[2s_{12}+2(s_{11}-s_{12})\tau_3^2]\}\frac{T}{2}\,,\\
\delta g_{xy}&=F_{66}(s_{11}-s_{12})(\tau_1^2-\tau_2^2)T+F_{64}\tfrac{1}{2}\sqrt{2}s_{44}(\tau_1+\tau_2)\tau_3 T\,.
\end{aligned} \tag{6}$$

The corresponding expressions for center B are obtained by a simple interchange of indices in the F_{ij}: $1\rightarrow2$, $2\rightarrow1$, $3\rightarrow3$, $4\rightarrow5$, $5\rightarrow4$, and $6\rightarrow6$. Expressions for centers C, D, E, and F are derived in an analogous way, but will not be reproduced here.

V. EXPERIMENTAL RESULTS

In a broad outline, our ESR results are in accord with those of Woodbury and Ludwig.[7] A salient distinction is the absence of the second, high-temperature axial Pt center. With respect to the low-temperature Pt center an additional detail in the superhyperfine structure was observed, which leads to a modification of the model of this center.

A. $\vec{\vec{g}}$ tensor

Angle-dependent spectra were taken with $\vec{H}$ rotating in the (001), (110), (111), and $(11\bar{2})$ planes. Six equivalent centers with spin $S=\frac{1}{2}$ are found. This implies that the site symmetry cannot be higher than

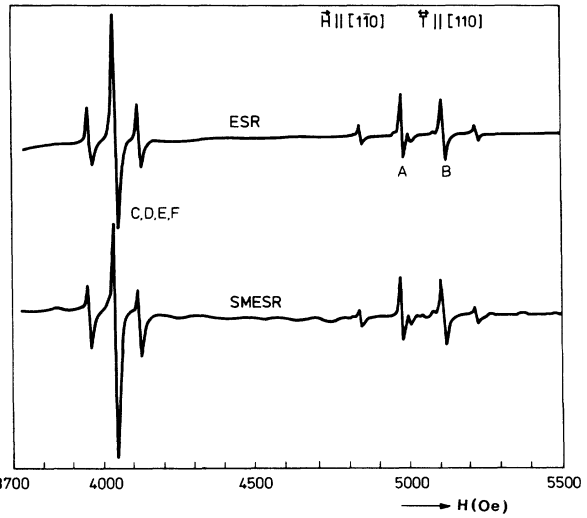

FIG. 1. Typical ESR and SMESR spectrum of Pt^- in Si for $\vec{H}||[1\bar{1}0]$ and $\vec{T}||[110]$. $\nu_0=9.9827$ GHz; $T=4.2$ K; microwave power $P_0=3$ mW. Lines are slightly distorted by (too) rapid scanning.

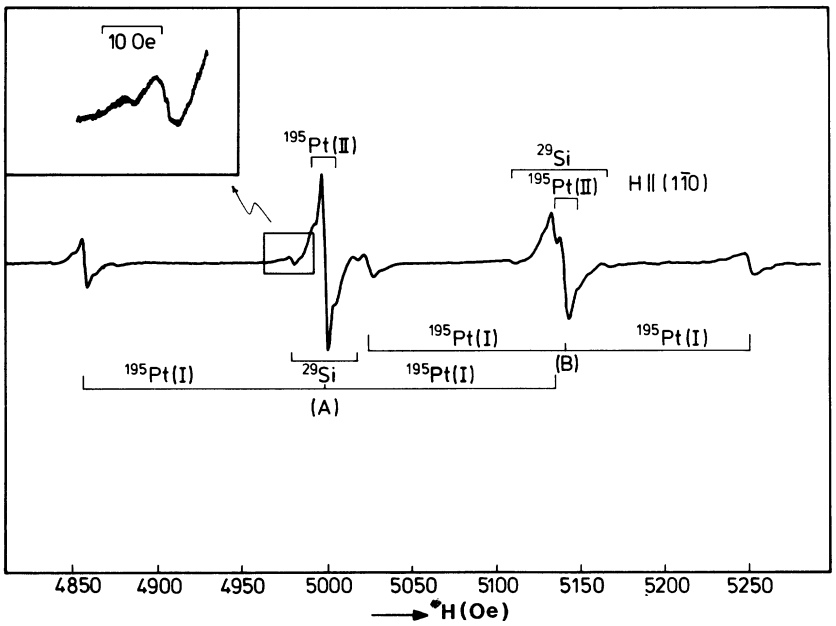

FIG. 2. Detail of ESR spectrum for $\vec{H}||[1\bar{1}0]$, showing hyperfine interactions with own ^{195}Pt nucleus, two neighboring ^{29}Si nuclei, and one distant ^{195}Pt nucleus.

orthorhombic. The line positions can be well fitted to an orthorhombic $\overleftrightarrow{g}$ tensor. The principal values of $\overleftrightarrow{g}$ agree well with those of Ref. 7, to within the quoted error margins. The linewidth is anisotropic and ranges from $\Delta H_d = 3.25$ Oe for $\vec{H}||[1\bar{1}0]$ to $\Delta H_d = 5.5$ Oe for $\vec{H}||[1\bar{1}1]$. A rough overview spectrum is shown in Fig. 1.

B. Hyperfine interaction with own ^{195}Pt

Since the natural mixture of Pt contains an odd isotope ^{195}Pt with $I = \frac{1}{2}$, in addition to a number of even isotopes (^{194}Pt, ^{196}Pt, ^{198}Pt with $I = 0$), a typical ESR transition consists of a triplet of lines. The central line is due to the even isotopes and the two outer lines represent the hyperfine interaction with the ^{195}Pt nucleus. They are indicated by ^{195}Pt(I) in Fig. 2. The natural abundance of ^{195}Pt is $\alpha = 0.338$, hence the intensity ratio of the triplet is $1{:}2(1-\alpha)/\alpha{:}1 = 1{:}3.9{:}1$. The principal axes of the hyperfine interaction coincide with those of the $\overleftrightarrow{g}$ tensor. The principal values are in good agreement with Ref. 7.

C. Hyperfine interaction with ^{29}Si

Superhyperfine structure due to the 4.7% abundant isotope ^{29}Si with $I = \frac{1}{2}$ is clearly distinguished (Figs. 2 and 3). The spectrum for $\vec{H}||[1\bar{1}0]$ shows unambiguously that the interaction is with two equivalent nearest-neighbor ^{29}Si nuclei. If the interaction were with four neighbors, two sets of satellites would be observed instead of one. This conclusion is corroborated by the observed intensity ratio satellite-main peak being equal to 0.048 ± 0.005, which compares favorably with the expected ratio $\alpha/(1-\alpha) = 0.049$, where α is the natural abundance.

The resolution of the superhyperfine structure (shfs) is not equally good for all $\vec{H}$ directions. This

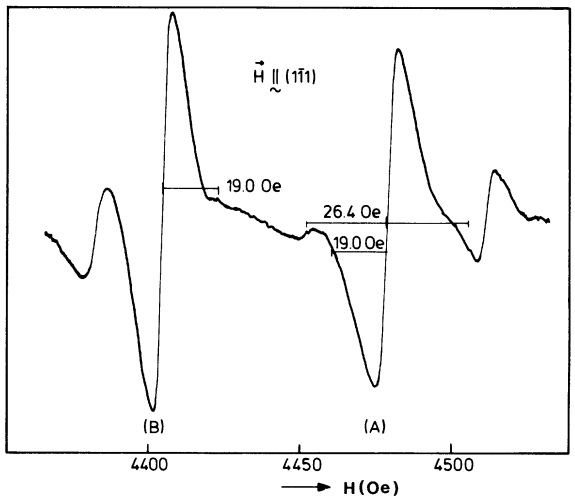

FIG. 3. Detail of ESR spectrum for $\vec{H}||[1\bar{1}1]$, showing ^{29}Si superhyperfine splittings. The stronger interaction (52.8 Oe) is with a ^{29}Si neighbor with shfs axis along $[1\bar{1}1]$; the smaller interaction (38 Oe) is with a ^{29}Si neighbor with shfs axis along $[\bar{1}11]$.

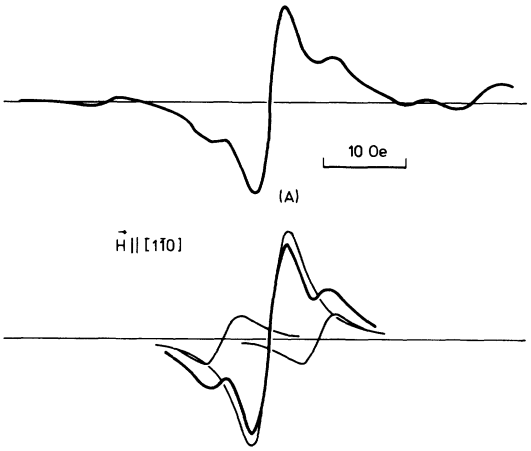

FIG. 4. Detail of line A in Fig. 2, showing hyperfine interaction with a distant ^{195}Pt nucleus (upper trace). Reconstruction of the central part of the line shape, assuming a natural abundance of 33.8%, $A_0/g\mu_B=11.50$ Oe, $\Delta H_d=4.25$ Oe (lower trace).

is partly due to the anisotropy of the linewidth and partly to coincidence of lines. The experimental data are sufficient, however, to conclude that the interaction tensor has axial symmetry along a ⟨111⟩ direction (±5°), with $|T_{\parallel}|=40.3\times10^{-4}$ cm^{-1} (±3%), $|T_{\perp}|=29.0\times10^{-4}$ cm^{-1} (±3%). Analysis of the experimental data was done using Eqs. (8) and (9) of Ref. 7. Our results are in reasonable agreement with the tentative data in Ref. 7. The signs of $T_{\parallel}$ and $T_{\perp}$ do not follow from the experiments, but most probably they are negative since the nuclear g_N value of ^{29}Si is negative.[8]

D. Hyperfine interaction with next-nearest-neighbor (NNN) ^{195}Pt

A glance at Fig. 2 clearly shows that, in addition to the splitting already mentioned, each line exhibits a further fine structure, indicated by ^{195}Pt(II). A more careful study of this structure (Fig. 4) shows that we have to do with a triplet similar to the ^{195}Pt hyperfine structure described in Sec. V B. A reconstruction, based on the intensity ratio 1:3.9:1, as dictated by the natural abundance of ^{195}Pt, leads to a satisfactory agreement with the observed shape (Fig. 4). The intensity of the satellites is obviously much too big to be accounted for by ^{29}Si hyperfine interactions. The hyperfine splitting is isotropic: $|A_0|=7.5\times10^{-4}$ cm^{-1} to within the limits of accuracy (±5%).

We attribute this additional splitting to an interaction with a second ^{195}Pt nucleus ($I=\frac{1}{2}$). The charge state of the second platinum is neutral; a negative charge state would lead to a completely different spectrum.[21,22] Instead of a triplet of triplets, as observed experimentally, we then would expect a more complicated structure consisting of a central triplet, with separation $\frac{1}{4}A^2/J_0$, surrounded by a doublet at $\pm\frac{1}{4}A$, with separation $\frac{1}{8}A^2/J_0$, and finally a singlet at $\pm\frac{1}{2}A$. Here J_0 means the isotropic exchange parameter of the Pt⁻-Pt⁻ pair.

The location of the second Pt^0 atom does not follow unambiguously from the hfs data, since A_0 is isotropic. A first-neighbor position, however, is incompatible with the orthorhombic symmetry of the g and A tensors. Additional data, related to the Pt^0 site, will be adduced in Secs. V G and V H.

E. Spin Hamiltonian

The spectral data, obtained thus far, can be summarized using the spin Hamiltonian

$$\mathcal{H}=\mu_B\vec{S}\cdot\overleftrightarrow{g}\cdot\vec{H}+\vec{S}\cdot\overleftrightarrow{A}\cdot\vec{I}+\sum_{k=1}^{2}\vec{S}\cdot\overleftrightarrow{T}_k\cdot\vec{I}_k+A_0\vec{S}\cdot\vec{I}\ . \tag{7}$$

The first term describes the Zeeman interaction of the unpaired electron spin ($S=\frac{1}{2}$); the second, third, and fourth terms represent the hyperfine interactions with the own ^{195}Pt nucleus ($I=\frac{1}{2}$), two ^{29}Si neighbors ($I_k=\frac{1}{2}$), and the distant ^{195}Pt nucleus ($I=\frac{1}{2}$), respectively. The parameters are given in Table II.

TABLE II. ESR results.

Center axes $\overleftrightarrow{g}$	$\overleftrightarrow{A}$ (own ^{195}Pt hfs)
$x=[1\bar{1}0]$ $g_x=1.3866\pm0.0002$	$\lvert A_x\rvert=150.5\times10^{-4}$ cm^{-1}
$y=[110]$ $g_y=1.4264\pm0.0002$	$\lvert A_y\rvert=184.8\times10^{-4}$ cm^{-1} (±1%)
$z=[001]$ $g_z=2.0789\pm0.0002$	$\lvert A_z\rvert=126.2\times10^{-4}$ cm^{-1}
$\overleftrightarrow{T}$ (^{29}Si hfs)	A_0 (NNN ^{195}Pt hfs)
$T_{\parallel}=-40.3\times10^{-4}$ cm^{-1}	$\lvert A_0\rvert=7.5\times10^{-4}$ cm^{-1} (±5%) (isotropic)
$T_{\perp}=-29.0\times10^{-4}$ cm^{-1} (±3%)	
hfs axis $=[111]$	

F. Number of active centers

The number of centers responsible for the Pt^- spectrum is determined by comparing the integrated intensity of the whole spectrum both with an internal (phosphorous donor) and with an external (Varian weak pitch) standard. Consistent results are obtained: $[Pt^-]=(4.8\pm0.5)\times10^{16}$ cm^{-3}. The total Pt content, as determined by neutron activation analysis, is twice as large: $[Pt]_{tot}=1.08\times10^{17}$ cm^{-3}. This is consistent with the idea that the ESR active centers are platinum pairs.

G. Strain dependence of $\overleftrightarrow{g}$

The recipe for the evaluation of the F-tensor elements is given in detail in Sec. IV. In essence, SMESR and ESR signal heights are compared for various orientations of stress axis $\vec{T}$ and magnetic field vector $\vec{H}$. First of all, we have to make sure what kind of stress-induced effect we are dealing with. It turns out that the major part ($>90\%$) of the SMESR response is in phase with the applied stress. Small out-of-phase signals (maximum 10% of the total signal height) occur when $\vec{T}$ is parallel to either [110] or [001]. For isolated lines the line shape of the in-phase signal is a symmetrical absorption derivative. Nearly coinciding lines, due to equivalent centers with distinct effective F values, may exhibit a slight asymmetry. *Grosso modo* we therefore conclude that we have to do with elastic shift SMESR [i.e., case (i) in Sec. IV] caused by modulation of the $\overleftrightarrow{g}$ tensor. Small anelastic effects are present, however. Their contribution is not evaluated explicitly, but is contained in the error margins quoted for the effective F values.

The strain-modulation amplitude used in the measurements ($\hat{e}_s\simeq0.5\times10^{-5}$) was low enough to avoid both breakaway of dislocations from their pinning points and modulation broadening of the resonance lines. A microwave power level of $P_0=3$ mW proved to be sufficiently low to avoid saturation at $T=4.2$ K. Anyway, for power levels between 0.03 and 10 mW, the effective F values proved to be independent of P_0.

Effective F_H^T values for various orientations of stress $\vec{T}$ and magnetic field $\vec{H}$ are given in Table III. As a rule, noncoinciding lines were used to determine F_H^T. For some orientations of $\vec{H}$, however, the resonance lines do coincide; in these cases the angular dependence of F_H^T was recorded and the extrapolated value was used. The data in Table III are corrected for passage effects (see Sec. IV). The signs of F_H^T were determined absolutely by going carefully through all phase shifts; an additional check was made by comparison with a standard sample ($MgO:Co^{2+}$), for which the signs are well known.[19,23]

The tensor elements F_{ij} are finally obtained by solving a set of linear equations, such as Eqs. (5) and (6). Twelve independent equations in the orthorhombic elements of $\overleftrightarrow{F}$ are obtained from the data points marked "orth." in Table III. The eight purely monoclinic tensor elements can be found from the data points marked "mon." As a rule, the latter are less accurate, the more so if they originate from small intensity differences between nearly coinciding lines. The remaining data are used to check the results and to arrive at a realistic estimate of the error margins.

In applying Eqs. (5) and (6) we used the elastic compliances of Si, as given by Landolt and Börnstein,[24] viz., $s_{11}=0.774\times10^{-12}$, $s_{12}=-0.217\times10^{-12}$, $s_{44}=1.26\times10^{-12}$ cm^2/dyn. It should be borne in mind that these are macroscopic elastic constants; hence the $\overleftrightarrow{F}$ tensor obtained here merely tells us what g shift can be expected for a given macroscopic deformation of the crystal.

The results are presented in Table IV. It turns out in an unambiguous way that an orthorhombic form of $\overleftrightarrow{F}$ is inadequate to describe the experimental data. A visual demonstration of this point is given in Fig. 5. Instead, the site symmetry proves to be monoclinic. The point group is C_s with the mirror plane (xz) as the only nontrivial symmetry element. It is also seen that the purely monoclinic elements are not small in comparison with the orthorhombic ones. This result seems to be at variance with the orthorhombic symmetry of the $\overleftrightarrow{g}$ tensor itself. Apparently, the magnetoelastic tensor $\overleftrightarrow{F}$ is a much more sensitive probe of the site symmetry than the spectroscopic splitting tensor $\overleftrightarrow{g}$. This is not astonishing, since line positions described by $\sum_k g_{ik}g_{jk}$ are known[25] to be rather insensitive to a descent in symmetry below orthorhombic. The monoclinic site symmetry, finally restricts the possible positions of the second Pt^0 atom to the (xz) mirror plane, which is the only nontrivial symmetry element of C_s.

H. Comparison of samples

All measurements described hitherto were done on float-zoned (FZ) n^+-type Si samples with $[P]=10^{18}$ cm^{-3}, $[Pt]=1.08\times10^{17}$ cm^{-3}, and $[O]=5\times10^{16}$ cm^{-3} (see Sec. III). Superficial ESR measurements on FZ samples with Pt concentrations down to 2×10^{16} cm^{-3} give identical results. We also made some additional ESR experiments on Czochralski (CZ) material with slightly lower phosphorous doping: $[P]=8.3\times10^{16}$ cm^{-3} and varying Pt contents $1.7\times10^{16}<[Pt]<6.6\times10^{16}$ cm^{-3}. The oxygen concentration in these samples is rather

TABLE III. SMESR data points.

Center	$\overleftrightarrow{T}$	$\vec{H}$	F_H^T	Symmetry[c]
A	110	001	−34.5±0.5	orth.
B	110	001	+98.5±2	orth.
A	110	$1\bar{1}0$	+20.0±2	orth.
B	110	$1\bar{1}0$	+21.0±1	orth.
A	110	$1\bar{1}1$	+9.8±2	mon.
B	110	$1\bar{1}1$	+44.8±5	
CDEF	110	001	−14.8±1	
CDEF	110	$1\bar{1}0$	+41.2±1	orth.
CE	110	$1\bar{1}1$	+28.2±1	
DF	110	$1\bar{1}1$	+24.2±1	
$\lvert C-E \rvert$[a]	110	$1\bar{1}1$	+5.4±3	mon.
$\lvert C-E \rvert$[a]	110	001	+4.0±3	mon.
$\lvert CE-DF \rvert$[a]	110	001	0 ±1	mon.
A	111	$1\bar{1}0$	−16.5±1	orth.
B	111	$1\bar{1}0$	+3.5±0.5	orth.
A	111	$11\bar{2}$	+21.0±2	orth.
B	111	$11\bar{2}$	+91.0±2	orth.
A	111	45°[b]	−5.5±2	mon.
B	111	45°[b]	+44.0±3	
CD	$11\bar{2}$	110	+43.9±2	mon.
EF	$11\bar{2}$	110	+51.9±2	mon.
A	$11\bar{2}$	111	+34.0±1	orth.
B	$11\bar{2}$	111	+11.6±1	orth.
CD	001	110	+20.3±1	orth. + mon.
EF	001	110	+22.2±1	orth. + mon.
A	001	110	−64.8±3	
B	001	110	−25.0±1	

[a]For $\vec{H}$ *near* specified axis.
[b]i.e., with direction cosines $(\sqrt{3}+6, \sqrt{3}-6, -2\sqrt{3})$.
[c]Data points marked orth. are used to determine the 12 orthorhombic elements of F; those marked mon. yield the 8 monoclinic elements.

high: $[O]=6\times10^{17}\ cm^{-3}$.

At first sight the ESR spectra of all samples look very much the same. To be more precise, the parameters of the spin Hamiltonian are identical within the accuracy limits of the experiments. There are, however, slight differences in the dynamical behavior of the resonance lines.

At $T=4.2$ K the ESR intensity of the FZ sample does not saturate up to a power level of $P_0=20$ mW. At $T=1.3$ K it shows a saturation behavior typical for inhomogeneously broadened lines.[26]

The ESR lines of the CZ samples, on the other hand, do saturate readily even at $T=4.2$ K. At $T=1.3$ K their saturation curves show a maximum around $P_0=30\ \mu$W and fall off to a nearly constant

TABLE IV. $\overleftrightarrow{F}$ tensor of $(Pt^-)_s$-$(Pt^0)_i$ pair in silicon.

Orthorhombic	Monoclinic
$F_{11}=-4\pm8$	$F_{15}=+182\pm10$
$F_{12}=-5\pm2$	$F_{25}=-182\pm10$
$F_{13}=-67\pm7$	$F_{35}=+117\pm30$
$F_{21}=+18\pm2$	$F_{46}=-78\pm15$
$F_{22}=+28\pm8$	$F_{64}=0\pm5$
$F_{23}=-12\pm7$	$F_{51}=+127\pm20$
$F_{31}=+172\pm4$	$F_{52}=+151\pm20$
$F_{32}=+47\pm4$	$F_{53}=-367\pm60$
$F_{33}=+193\pm7$	
$F_{44}=+8\pm4$	
$F_{55}=-5\pm4$	
$F_{66}=-1\pm5$	

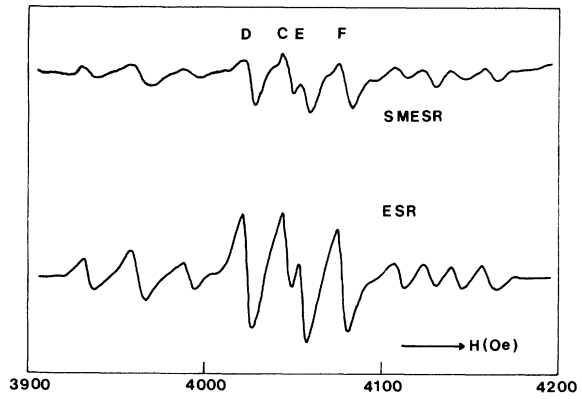

FIG. 5. Detail of SMESR and ESR spectrum for $\vec{T}[110]$ and $\vec{H}\|[1\bar{1}0]$ ($\simeq 10°$ misorientation). For orthorhombic site symmetry the intensity ratios I (SMESR)/I (ESR) should be identical for centers D, C, E, and F. The observed ratios 0.39, 0.45, 0.30, and 0.41 (± 0.02) clearly indicate that the symmetry is lower than orthorhombic.

value at high powers.

In all samples studied, the temperature dependence of the ESR intensity follows a perfect $1/T$ law (measured for $1.2 < T < 4.2$ K). Finally, no indications of double quantum transitions are found at high microwave powers (up to $P_0 = 100$ mW). Thus the resonance arises from a ground-state doublet ($S = \frac{1}{2}$) in all samples. Pt^--Pt^- pairs, with $S = 1$ or 0, have not been observed. Neither do we find any trace of isolated Pt^- ions. Our conclusion, therefore, is that the Pt^--Pt^0 center is a well-defined magnetic complex in n-type silicon. Its static spin-Hamiltonian parameters are not sample dependent.

A very important result is the absence of Pt^--Pt^- pairs, even in samples with [P]/[Pt] ratios as large as 10. This means that the two Pt atoms are at distinct types of sites, e.g., one at a (near) substitutional and the other one at an interstitial site. It is well known that transition metals at interstitial sites in Si can act as donors, but not as acceptors.[6] The occurrence of Pt^+-Pt^+ pairs[12] in p^+-type Si is therefore compatible with this picture.

VI. DEDUCTION OF A MODEL

The experimental data, collected hitherto, allow the construction of a geometrical model of the Pt center in silicon. Some remarks can also be made concerning the wave function of the complex.

The stability of the Pt^--Pt^0 center is high. Samples prepared five years ago still give the same ESR spectrum without measurable loss of intensity. This suggests that at least one of the Pt atoms is at or near a substitutional position.[6,7] If Pt^- were exactly at a substitutional site, hyperfine interaction with four equivalent silicon neighbors would be expected. As a matter of fact, we observe a ligand hyperfine structure due to only two equivalent ^{29}Si nuclei. This means that Pt^- forms chemical bonds with two neighboring Si atoms. The other two Si neighbors form a so-called reconstructed bond. The inequivalency of the four Si neighbors may be provoked by a shift of the Pt^- ion along a [001] direction. This picture leads to a C_{2v} symmetry for the $[PtSi_4]^-$ complex. The form of the magnetoelastic tensor $\overleftrightarrow{F}$, however, definitely reveals a monoclinic site symmetry. This lowering of symmetry must be related to the presence of the second Pt atom. From an analysis of the hyperfine pattern it follows unambiguously that this second platinum is in the neutral charge state Pt^0. A comparison of samples with widely varying [P]/[Pt] ratios shows that the charge state Pt^--Pt^- does not occur. This implies that the second Pt atom cannot be at a substitutional site, where it would be amphoteric. Transition metals at interstitial sites, on the other hand, are known to act as donors only. In principle, many interstitial sites are feasible in the silicon lattice; the C_s symmetry of the center restricts the positions of Pt^0 to the mirror plane (xz). Figure 6 visualizes the geometrical model of the $(Pt^-)_s$-$(Pt^0)_i$ center, as deduced from the foregoing arguments.

In the next few paragraphs we will explore what qualitative conclusions can be drawn concerning the nature of the odd-electron wave function ψ_0. The hyperfine interaction with only two Si neighbors

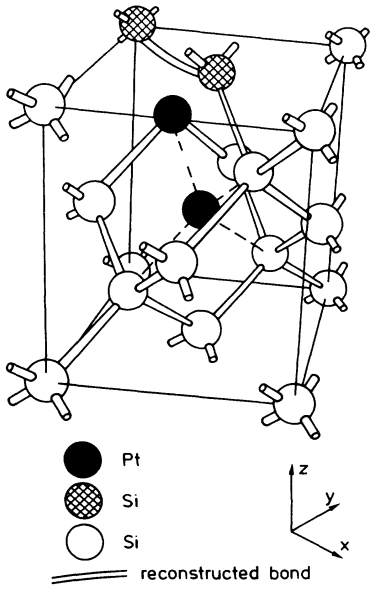

FIG. 6. Proposed model of the Pt center in Si.

suggests the presence of a reconstructed bond, analogous to the silicon A center.[8,9] This analogy was also stressed by Lowther's cluster calculations.[10] In the A center the odd electron moves in an antibonding orbital of the reconstructed Si—Si bond. Since this orbital has a node at the central oxygen position, ^{17}O hyperfine structure is missing.

The analogy between the Pt^--Pt^0 center and the A center is far from being perfect. The first contradistinction is found in the magnitude of the spin density at the Si sites. If we decompose the experimental $T_{||}$ and $T_\perp$ values (Table II) into an isotropic part

$$a=(16\pi/3)g_N u_B u_N f_s |\psi_{3s}(0)|^2 = -32.7\times10^{-4},$$

in units of cm^{-1}, and a quasidipolar part

$$b=\tfrac{4}{5}g_N u_B u_N f_p \langle r^{-3}\rangle_{3p} = -3.7\times10^{-4},$$

in units of cm^{-1}, we find $f_s=0.031$ and $f_p=0.103$ using $|\psi_{3s}(0)|^2=24\times10^{24}$ cm^{-3} and $\langle r^{-3}\rangle_{3p}=17\times10^{24}$ cm^{-3}.[8] The s-spin density f_s in the A center is a factor of 4 larger than the value quoted here. Thus, in the Pt^--Pt^0 center, only a minor part of the spin density is near the Si nuclei. The ratio $f_p/f_s=3.36$ shows that the silicon bonding orbitals σ_i are practically pure sp^3 hybrids. In the A center a much greater deviation from sp^3 hybridization was detected: $f_p/f_s=1.70$.

Another point of contrast with the A center is the rather large value of the central ^{195}Pt hyperfine interaction. In C_s symmetry the interpretation of the isotropic part $|\mathcal{A}|=153.8\times10^{-4}$ cm^{-1} is complicated by the fact that it may arise both from spin polarization of inner ns shells and from direct mixing of $6s$ and $6p_z$ orbitals (which transform according to the same irreducible representation A_1 of C_s). Anyway, it is obvious that the spin density near the Pt^- nucleus is quite high and that Pt^- orbitals must be involved in ψ_0. The fact that the hyperfine interaction with the second Pt^0 atom is purely isotropic suggests the presence of at least a small fraction of Pt^- ($6s$) character in ψ_0.

Further information about the nature of the Pt^- orbitals involved in ψ_0 is provided by the g tensor and its strain dependence $\overleftrightarrow{F}$. The value of $g_{zz}=2.0789$, close to the free-electron g factor, suggests that the odd electron is either in a $5d_{z^2}$ or in a $6p_z$ orbital of Pt^-; for both of them we have $L_z|d_{z^2}\rangle=0$, $L_z|p_z\rangle=0$. We prefer the latter for the following reasons.

In the former case the paramagnetism arises from the Pt $5d$ shell [configuration $5d^9$, case (iii) in Sec. I]. The reconstructed Si—Si bond is filled with two electrons. Ligand hyperfine structure presumably arises from the two Si atoms chemically bonded to Pt^-. The spin density at the Si site $f_s=0.031$ is not in disaccord with this model.[27] A serious objection is the fact that the odd electron of a $5d^9$ configuration in fourfold coordination is not expected to occupy a d_{z^2} orbital. Instead, one of the t_2 orbitals (d_{xz}, d_{yz}, or d_{xy}) would be preferred. It is not to be expected that the presence of the interstitial $(Pt^0)_i$ atom reverses completely the order of the d levels of $(Pt^-)_s$.

In the preferred model, the platinum $6p_z$ orbital is thought to form a very weak bond with the symmetrical combination $(\sigma_3+\sigma_4)$ of σ orbitals of the reconstructed bond. This gives rise to a bonding and an antibonding state, which lie close together in the forbidden zone. As in the A center, the bonding orbital is filled with two electrons and the odd electron occupies the antibonding state. The d shell is filled with eight electrons, which are paired off. This is, in fact, a slightly modified form of case (ii) in Sec. I. The proposed form of ψ_0 is then

$$\psi_0=N[(6p_z)_{Pt}+\alpha(6s)_{Pt}+\beta(6p_x)_{pt}-\gamma(\sigma_3+\sigma_4)], \tag{8}$$

with $\alpha,\beta,\gamma<1$. The term $\beta(6p_x)$ is allowed in C_s symmetry and is needed to explain the strain dependence of $\overleftrightarrow{g}$. According to the theory of Mattuck and Strandberg,[28] the strain-induced change of the g tensor of an electronically nondegenerate system is given by a third-order cross effect of spin-orbit interaction, Zeeman interaction, and orbit-lattice interaction:

$$\delta g_{ij}=\frac{1}{\Delta E_{n0}\Delta E_{k0}}\sum_n\sum_k\langle 0|\lambda L_i|n\rangle\langle n|L_j|k\rangle\langle k|\sum_p V_p e_p|0\rangle+\text{permutations}. \tag{9}$$

Since $L_z|p_z\rangle=0$, $L_z|s\rangle=0$ we would expect a vanishing value of δg_{zz} for all strain components e_p. Experimentally we find that F_{31}, F_{32}, and F_{33} belong to the largest elements of the $\overleftrightarrow{F}$ tensor. This can only be explained if some $6p_x$ admixture into ψ_0 is admitted. A final point in favor of this model is the similarity of the electron-capture cross sections of the A center[29] ($\sigma_n=10^{-14}$ cm^2) and the Pt^--Pt^0 center[4] ($\sigma_n=7\times10^{-15}$ cm^2). These extremely large values of σ_n can hardly be reconciled with a $5d^9$ configuration.

ACKNOWLEDGMENTS

The authors are indebted to S. D. Brotherton, who raised their interest in the Si:Pt problem and provided the samples. Neutron activation analysis was carried out by M. L. Verheyke and H. J. J. Jaspers. J. P. M. Ansems skillfully assisted during the final stage of the experiments and P. C. M. Baken was responsible for the oxygen determination. Finally, R. P. van Stapele was kind enough to carefully read the manuscript and to eliminate several inconsistencies in the mathematics.

---

[1]W. M. Bullis, Solid-State Electron. 9, 143 (1966).
[2]D. V. Lang, H. G. Grimmeiss, E. Meijer, and M. Jaros, Phys. Rev. B 22, 3917 (1980).
[3]S. Braun, H. G. Grimmeiss, and K. Span, J. Appl. Phys. 48, 3883 (1977).
[4]S. D. Brotherton, P. Bradley, and J. Bicknell, J. Appl. Phys. 50, 3396 (1979).
[5]S. D. Brotherton and J. E. Lowther, Phys. Rev. Lett. 44, 606 (1980).
[6]G. W. Ludwig and H. H. Woodbury, in *Solid State Physics,* edited by F. Seitz and D. Turnbull (Academic, New York, 1962), Vol. 13, p. 223.
[7]H. H. Woodbury and G. W. Ludwig, Phys. Rev. 126, 466 (1962).
[8]G. D. Watkins and J. W. Corbett, Phys. Rev. 121, 1001 (1961).
[9]J. W. Corbett, G. D. Watkins, R. M. Chrenko, and R. S. MacDonald, Phys. Rev. 121, 1015 (1961).
[10]J. E. Lowther, J. Phys. C 13, 3665 (1980); 13, 3681 (1980).
[11]J. C. M. Henning and J. H. den Boef, Phys. Rev. B 18, 60 (1978).
[12]J. C. M. Henning and E. C. J. Egelmeers, Solid State Commun. 38, 1037 (1981).
[13]Y. G. Badalian and V. F. Kazantsev, in *Proceedings of the 7th International Congress on Acoustics, Budapest (1971)* (Akademiai Kiadó, Budapest, 1971), Vol. 4, p. 225.
[14]M. A. Collins, S. D. Devine, R. A. Hoffman, and W. H. Robinson, J. Phys. C 4, L116 (1971); J. Magn. Reson. 6, 376 (1972).
[15]J. C. M. Henning and J. H. den Boef, Phys. Lett. 46A, 183 (1973).
[16]J. Wosik, K. Nesteruk, W. Zbieranowski, and A. Sienkiewicz, J. Phys. E 11, 1200 (1978).
[17]S. Maekawa and N. Kinoshita, J. Phys. Soc. Jpn. 20, 1447 (1965).
[18]S. D. Brotherton (private communication).
[19]J. C. M. Henning and J. H. den Boef, Phys. Rev. B 14, 26 (1976).
[20]W. G. Cady, *Piezoelectricity* (Dover, New York, 1964), Chap. IV.
[21]J. W. Culvahouse, D. P. Schinke, and L. G. Pfortmiller, Phys. Rev. 177, 454 (1969).
[22]J. C. M. Henning, in *Ampère International Summer School II Pulsed Magnetic and Optical Resonance, Basko Polje, Yugoslavia, 1971,* edited by R. Blinc (Institute Jošef Stefan and University of Ljubljana, Ljubljana, 1972), p. 179.
[23]E. B. Tucker, Phys. Rev. 143, 264 (1966).
[24]H. H. Landolt and R. Börnstein, *Numerical Data,* edited by K. H. Hellwege (Springer, Berlin, 1969), Vol. III 2.
[25]A. B. Roitsin, Phys. Status Solidi B 104, 11 (1981).
[26]C. P. Poole and H. A. Farach, *Relaxation in Magnetic Resonance* (Academic, New York, 1971), Chaps. 13 and 15.
[27]J. Owen and J. H. M. Thornley, Rep. Prog. Phys. 29, 676 (1966).
[28]R. D. Mattuck and M. W. P. Strandberg, Phys. Rev. 119, 1204 (1960).
[29]L. C. Kimerling, IEEE Trans. Nucl. Sci. NS-23, 1497 (1976).